Impedance statistics of cable networks that model quantum graphs

Tornike Ghutishvili[*]
Department of Physics, University of Maryland, College Park, Maryland 20742, USA

Lei Chen[†] and Steven M. Anlage[‡]
Maryland Quantum Materials Center, Department of Physics, University of Maryland, College Park, Maryland 20742, USA and Department of Electrical and Computer Engineering, University of Maryland, College Park, Maryland 20742, USA

Thomas M. Antonsen[§]
Department of Physics, University of Maryland, College Park, Maryland 20742, USA and Department of Electrical and Computer Engineering, University of Maryland, College Park, Maryland 20742, USA

(Received 12 December 2022; accepted 14 July 2023; published 18 September 2023)

We present the theoretical framework required to describe the statistics of microwave networks that serve to model quantum graphs. The networks are described by impedance and admittance matrices relating the voltages and currents at the network's ports. As we show, these matrices can be calculated in a number of ways. Normal modes of the network are characterized by a discrete set of wave numbers corresponding to the propagation constants on the network's bonds for which the determinant of the admittance matrix vanishes. The distribution of the spacings between adjacent eigenmode wave numbers is found to depend on the nature of the way bonds are connected at nodes. The critical quantity is the reflection coefficient presented at a node to a wave on a bond. As the reflection coefficient increases, the spacing distribution changes from one characteristic of the spacing of eigenvalues of a Gaussian orthogonal ensemble matrix to a Poisson distribution. The effect of loss is studied, and the scaling of the variance of the impedance values on network size, degree distribution, and other parameters is characterized. We attempted to find universal scaling relations for the distribution of impedance values for networks of different sizes. Finally, we compare the distribution of impedance values predicted by the model with those measured in a network of cables.

DOI: 10.1103/PhysRevResearch.5.033195

I. INTRODUCTION

In this paper, we investigate the properties of electrical networks that model quantum graphs. The term "quantum graph" refers to a system in which waves propagate along one-dimensional paths that meet at junctions, where the waves interfere and interact. Due to their simplicity, involving one-dimensional wave propagation only, quantum graphs have been used extensively as a simple model to analyze and understand a variety of wave systems [1–6]. Examples include quantum wires [7,8], mesoscopic quantum systems [9], electromagnetic waveguide networks [10–12], and others.

This type of model was first used by Pauling [13], who introduced a quantum graph model to describe the behavior of itinerant electrons in organic molecules. The word "quantum" in the name comes from the fact that the system is described by a wave equation, similar to the one-dimensional Schrödinger equation, and thus it has a discrete set of eigenmodes and frequency eigenvalues. It has been shown [14] that the eigenvalue spectra of isolated quantum graphs with incommensurable bond lengths have statistical properties that are described by random matrix theory (RMT) [15]. Quantum graphs are divided into orthogonal, unitary, and symplectic universality classes. All of them can be realized experimentally with microwave networks. Quantum graphs with time-reversal invariance have spectral properties similar to random matrices drawn from Gaussian orthogonal ensembles (GOEs). Such systems are realized experimentally by networks of transmission lines connected at nodes characterized by symmetric scattering matrices [12]. Quantum graphs without time-reversal invariance have properties similar to random matrices drawn from a Gaussian unitary ensemble (GUE). Such networks are realized experimentally with the insertion of circulators in the transmission lines [16–21]. Quantum graphs with spectra described by Gaussian symplectic ensembles (GSEs) can be approximately realized by constructing graphs with symmetric paths and circulators [16,22,23].

This paper contains work only on time-reversal invariant systems, which have been extensively studied experimentally

[*]tornike@umd.edu
[†]lchen95@umd.edu
[‡]anlage@umd.edu
[§]antonsen@umd.edu

[19–21,24–28]. The main focus is the study of the statistics of the system's eigenmodes and the statistics of the elements of the network's impedance matrix. The eigenmodes of the system are labeled by index n and have propagation wave numbers on the bonds k_n. We study the spacing distribution of these wave numbers, and we find that in cases in which the reflection coefficients at the nodes are low, the distribution of spacings is characteristic of a time-reversal symmetric, wave chaotic system. This is similar to earlier findings [19,27,29]. Additionally, we have studied how the spacing distribution can be altered by changing scattering matrices at the nodes. In particular, as the reflection coefficients at the nodes are increased, the spacing distributions approach that of an integrable wave system.

To derive results for the impedance matrix, we treat the system as an electrical network that is characterized by a linear, frequency-dependent matrix that relates the voltages at the nodes of the system to the currents injected at the nodes. The impedance matrices of networks modeled as quantum graphs have been studied previously [1,12,30–33]. In this paper, we first derive three different approaches to calculate the impedance matrix of the system, and we show that they agree. We subsequently compare numerical predictions for the elements of the impedance matrices with measurements made in the laboratory, and we find agreement. We confirm that the impedance matrix statistics do not agree with those of two- and three-dimensional cavities, which are well described by the random coupling model (RCM) [34–39]. Finally, we investigate the change in the statistical properties as propagation loss along the bonds is increased. We find a new scaling for the statistics as a function of propagation loss as the size of the network is increased.

II. NETWORK MODEL

In this section, we present a model of a quantum graph in the form of a network of transmission lines. We will consider both the normal modes of the undriven network (the eigenmodes) and the case of the network driven by an injected signal. In the first case, we will examine statistics of the network's eigenvalues (resonant frequencies) and eigenfunctions (network voltages). In the second case, we will examine the linear relation between injected signals and network voltages. We will show how these two situations are related. Additionally, we will introduce several ways of calculating the matrices that describe the network.

As our model of a graph, we consider the network shown in Fig. 1. It consists of lengths of transmission lines (the bonds) that connect at junctions (the nodes) that are labeled $i = 1, N$. Such graphs are called metric graphs [2]. We adopt a simple model of the nodes in which the voltage at each node has a single value V_i, and the currents entering the node can pass to the ground through an element with complex impedance, Z_i. Moreover, node-i may be connected by a bond, which we treat as a transmission line, to node-j. In our studies, we have used this simple model for the nodes. A consequence is that all nodes reflect signals incident on the node from a bond to some degree. Others [2,32,40] have considered so-called Fourier nodes for which the reflection coefficient can be set to zero. This gives added freedom in terms of network properties

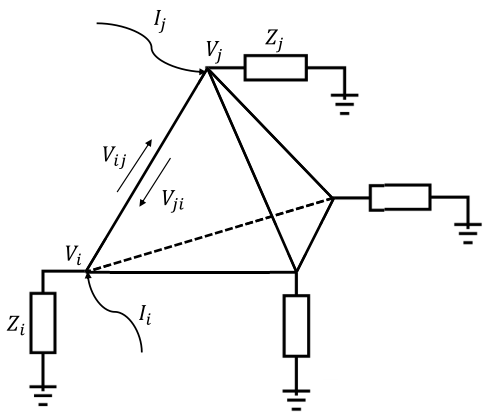

FIG. 1. A schematic representation of a tetrahedral network with four nodes and six bonds. At the node where the bonds meet a complex impedance to ground, Z_i is added. Note that the network is open to infinite leads at nodes i and j.

and increases the ability to recover the RCM statistics. However, such nodes are not easily constructed in practice, so we confine our studies to the simple nodes pictured in Fig. 1.

We assume the voltages and currents on the transmission lines satisfy the frequency domain version of the Telegrapher's equations,

$$ikV(z) = Z_0 \frac{\partial I(z)}{\partial z}, \tag{1a}$$

$$ikZ_0 I(z) = \frac{\partial V(z)}{\partial z}, \tag{1b}$$

where the propagation constant $k = \omega/v$, where ω is the angular frequency, v is the propagation speed, and Z_0 is the characteristic impedance of the transmission line. We note that the characteristic impedance may be removed from the problem by defining a new variable $[Z_0 I(z)]$. We keep it here to connect to real networks consisting of sections of a transmission line. Initially, we take the propagation constant to be real. Subsequently, we will consider dissipation on the line in which case $k = \omega/v + ik_{\rm im}$, where $k_{\rm im}$ is a damping rate. For simplicity, we assume all the transmission line properties are identical from a bond to a bond except for their lengths $L_{ij} = L_{ji}$.

The transmission lines carry waves propagating in both directions along each transmission line with propagation constant k. We label the amplitude of the voltage wave traveling from node-i and propagating to node-j as V_{ij}. This is the amplitude of the voltage wave as it leaves node-i. The voltage satisfying the Telegrapher's equations as a function of distance z from node-i can then be written

$$V(z) = V_{ij} e^{ikz} + V_{ji} e^{-ik(z-L_{ij})}. \tag{2}$$

Note that the voltage a distance z' from node-j can be found either by the replacement $z \to L_{ij} - z'$ or by the interchange of indices i and j. Using Eq. (2), we can express the node voltage in terms of the wave amplitudes V_{ij},

$$V_i = V_{ij} + V_{ji} e^{ikL_{ij}}, \tag{3a}$$

$$V_j = V_{ji} + V_{ij} e^{ikL_{ij}}. \tag{3b}$$

From these equations, we can derive expressions for the wave amplitudes in terms of the node voltages:

$$V_{ij} = \frac{i\left(e^{-ikL_{ij}}V_i - V_j\right)}{2\sin(kL_{ij})}, \tag{4a}$$

$$V_{ji} = \frac{i\left(e^{-ikL_{ij}}V_j - V_i\right)}{2\sin(kL_{ij})}. \tag{4b}$$

Associated with the voltage waves are current waves, which, according to Eqs. (1b) and (2), can be written as

$$I(z) = \frac{1}{Z_0}\left(V_{ij}e^{ikz} - V_{ji}e^{-ik(z-L_{ij})}\right), \tag{5}$$

where again Z_0 is the characteristic impedance of the transmission line. This expression represents the current flowing on the line in the $+z$ direction. Thus, the current leaving node-i in the direction of node-j is

$$\begin{aligned} I_{i\to j} &= \frac{1}{Z_0}\left(V_{ij} - V_{ji}e^{ikL_{ij}}\right) \\ &= \frac{i}{Z_0\sin(kL_{ij})}[V_i\cos(kL_{ij}) - V_j], \end{aligned} \tag{6}$$

where we have used Eqs. (4) to express the voltage wave amplitudes in terms of the node voltages.

We now apply Kirchhoff's current law to node-i. We imagine there is a current source injecting a current I_i into node-i. This current must balance all the other currents leaving node-i, either through the transmission line bonds or through the impedance Z_i to ground,

$$\begin{aligned} I_i = \sum_{j\neq i} I_{i\to j} + \frac{V_i}{Z_i} &= V_i\left(\frac{1}{Z_i} + \frac{i}{Z_0}\sum_{j\neq i}\frac{\cos(kL_{ij})}{\sin(kL_{ij})}\right) \\ &- \frac{i}{Z_0}\sum_{j\neq i}\frac{V_j}{\sin(kL_{ij})}. \end{aligned} \tag{7}$$

Here it is understood that the sum over j is only over those nodes that share a bond with node-i. Relation (7) can be cast in the form of an admittance matrix,

$$I_i = \sum_j Y_{ij}(k)V_j, \tag{8}$$

where

$$Y_{ii} = \left(\frac{1}{Z_i} + \frac{i}{Z_0}\sum_{j\neq i}\frac{\cos(kL_{ij})}{\sin(kL_{ij})}\right) \tag{9a}$$

and

$$Y_{ij} = -\frac{i}{Z_0\sin(kL_{ij})}, \quad j \neq i. \tag{9b}$$

The inverse of this admittance matrix is an impedance matrix,

$$V_i = \sum_j Z_{ij}(k)I_j. \tag{10}$$

This situation described in Eq. (7), where the voltages at the ends of the edges that are common to a node are equal, and the current entering the node flows to the ground through an impedance Z_i, corresponds to a special case of the boundary conditions considered in Ref. [41]. Specifically, the boundary condition may be cast in the general form $\mathbf{A}V + \mathbf{B}V' = 0$, where $\mathbf{A}$ and $\mathbf{B}$ are d by d square matrices, and V and $V' = dV/dz$ are d-dimensional vectors. Here d is the degree of the node in question, and the elements of V and V' are the voltages and their derivatives evaluated on the end of the edges connected to the node in question. In the case here, $\mathbf{B}$ takes the form $\mathbf{B} = \mathrm{i}(\mathrm{k}Z_0)^{-1}\mathbb{1}\mathbb{1}^{\mathsf{T}}$, with $\mathbb{1}$ being a d-dimensional vector whose elements are all unity, and superscript T implies transpose. More simply, $\mathbf{B}$ is a matrix whose elements are all equal. The matrix $\mathbf{A}$ takes the form $\mathbf{A} = Z_i^{-1}\mathbf{I}$, where $\mathbf{I}$ is the identity matrix. This boundary condition is chosen for two reasons. First, it can be easily implemented in an experiment. Second, by choosing the impedance Z_i to be reactive, the scattering matrix for a node is unitary and the diagonal elements can be adjusted. We will explore the consequences of this in the next section.

In the next sections, we will investigate the properties of these matrices for networks of varying complexity. Before doing that, we will derive an expression for the impedance matrix in terms of the normal modes of a network.

Normal modes of the system are found for values of the propagation constant $k = k_n$ for which the node voltages are nonzero in the absence of injected current. This corresponds to setting the determinant of the admittance matrix to zero,

$$\det\left(Y_{ij}(k_n)\right) = 0. \tag{11}$$

The discrete propagation constants k_n will be real in the absence of losses, $k_{\mathrm{im}} = 0$ and $\mathrm{Re}(Z_i) = 0$. Further, if the load impedance is independent of frequency, $dZ_i/d\omega = 0$, all mode energy is stored on the bonds. In this case, we expect the average spacing in wave numbers between modes to be determined by the total length of the bonds, $\langle k_{n+1} - k_n\rangle = \pi/L_T$, where $L_T = \sum_{ij} L_{ij}$. This relation will be checked when we solve various network realizations numerically.

The energy stored on a bond is the sum of the electric and magnetic field energy of the waves on the transmission line constituting the bond,

$$\begin{aligned} U_{ij}^{(n)} &= \frac{1}{v}\int_0^{L_{ij}} dz\left(Z_0^{-1}\frac{|V^{(n)}(z)|^2}{2} + Z_0\frac{|I^{(n)}(z)|^2}{2}\right) \\ &= \frac{2L_{ij}\left|V_{ij}^{(n)}\right|^2}{vZ_0}. \end{aligned} \tag{12}$$

Here we have made use of the fact that the network is time-reversal symmetric, and as a consequence, $|V_{ij}^{(n)}| = |V_{ji}^{(n)}|$. Also, we now use a superscript (n) to denote a voltage or current value associated with the normal mode of the undriven network having propagation constant k_n. When we solve for the modes of the network, we will normalize the node voltages such that each mode has the same total energy, $U_T^{(n)} = \sum_{ij} U_{ij}^{(n)}$.

There is a relation between the normal modes and the impedance matrix, which for a driven system $I_j \neq 0$ is defined for all values of propagation constant k (see Appendix A),

$$Z_{ij} = \sum_n \frac{iV_j^{(n)}V_i^{(n)*}}{(k-k_n)vU_T^{(n)}}. \tag{13}$$

Here $V_i^{(n)}$ is the voltage amplitude at node-i for mode n, $U_T^{(n)} = \sum_{ij} U_{ij}^{(n)}$, where $U_{ij}^{(n)}$ is given by Eq. (12). It should be noted for this system that the sum is over modes with both positive and negative values of k_n and that the node voltages for the modes are real. This gives the elements of the impedance matrix the property that for real k, they are imaginary and odd functions of k. Further, if we give $k = \omega/v$ a small positive imaginary part, the real parts of the diagonal elements of the impedance matrix are positive as demanded by causality. This expression will be compared with direct inversion of the admittance matrix, Eqs. (9a) and (9b), in the next section.

There is also a third way to calculate the impedance matrix based on summing contributions from the different paths a signal may take in traversing the graph. Specifically, we can express elements of the impedance matrix in the following way. For diagonal elements, we write

$$Z_{ii,\text{path}} = Z_{\text{in},i}\left[1 + \sum_{\text{paths}} \prod_{\text{Bonds}} \sigma_b e^{i\theta_b}\right], \tag{14}$$

and for off-diagonal elements, we write

$$Z_{ij,\text{path}} = Z_{\text{in},i} \sum_{\text{paths}} \prod_{\text{Bonds}} \sigma_b e^{i\theta_b}. \tag{15}$$

Here the sum over paths is a sum over all paths starting and ending at node-i in the case of the diagonal elements and starting at node-i and ending at node-j in the case of the off-diagonal elements. The products are over the bonds that constitute the steps in the paths. On each bond, a phase factor $\theta_b = kL_b$ is accumulated, where L_b is the length of the bond. The factors σ_b that are also accumulated are determined by how the path is followed from one bond to the next. If the signal is reflected at the end of a bond and then retraces the same bond, the factor is given by $\sigma_b = \rho_b$, where ρ_b is the voltage reflection coefficient at the node where the reflection occurs. If the signal passes through the node to a different bond, then $\sigma_b = 1 + \rho_b$, which is the voltage transmission coefficient. The voltage reflection coefficient depends on the number of bonds connected to a node and the impedance Z_j that is connected to the ground at that node. Let us define the equivalent impedance to the ground of a node, which is connected to N_j bonds,

$$Z_{\text{eq},j}^{-1} = Z_j^{-1} + (N_j - 1)Z_0^{-1}. \tag{16}$$

This is the impedance seen by a wave incident on one bond due to the load and the other bonds. It is the parallel combination of the load to ground Z_j and the $N_j - 1$ other bonds. The voltage reflection coefficient is then

$$\rho_b = \frac{Z_{\text{eq},j} - Z_0}{Z_{\text{eq},j} + Z_0}. \tag{17}$$

When a path ends on a node, which is considered to be a port, then the factor $\sigma_b = 1 + \rho_b$ is applied as if the signal were passing to another bond. The input impedance at the node is the parallel combination of the load impedance Z_j and the N_j transmission lines forming the bonds,

$$Z_{\text{in},j}^{-1} = Z_j^{-1} + N_j Z_0^{-1} = Z_{\text{eq},j}^{-1} + Z_0^{-1}. \tag{18}$$

It can be shown that with these definitions, each term in the sum for off-diagonal impedance elements satisfies the reciprocity condition $Z_{ij} = Z_{ji}$.

In principle, the sum over paths gives the exact value of an element of the impedance matrix only when an infinite number of paths is considered. However, useful approximations to the value of an impedance element can be obtained with a finite number of paths in two cases. The first case is if the network has a loss, either in the transmission lines or the loads to the ground. In this case, signals are attenuated fast enough as they propagate so that the size of the individual terms in the sum over longer and longer paths decreases faster than the number of such paths increases. The second case is the one in which the sliding window average using the Lorentzian weighting function is sought rather than the precise value at a given frequency. Averaging over a window of frequencies (or wave numbers) of width Δk, in this way, is equivalent to adding loss $k_{\text{im}} = \Delta k$, and it causes the contribution of paths of length L to decrease as $\exp(-\Delta k L)$.

III. NUMERICAL ANALYSIS OF THE GRAPHS

In the previous section, we discussed the theoretical framework necessary to study network graphs. Now, we numerically analyze different graphs. The first graphs we choose are the tetrahedron graph, which has four nodes and three bonds per node, and a larger graph, which has 16 nodes and three bonds per node. We examine the properties of the eigenfunctions and the eigenvalues for these graphs. Recall that the eigenvalues are the set of propagation constants k_n for which Eq. (8) has solutions with all injected currents I_i set to zero. For each propagation constant k_n, we find a set of node voltages, which we normalize according to Eq. (12).

For the tetrahedron graph, with the set of bond lengths (1.45, 1.67, 3.05, 3.57, 4.42, and 4.67), we select $M = 2990$ eigenfunctions in sequence with eigenvalues $k_1 - k_M$ spanning the range $k_1 = 0.57$ to $k_M = 499.95$. The average spacing of eigenvalues for the $N = 4$ graph is $\langle k_{n+1} - k_n\rangle = (k_M - k_1)/(M - 1) = 0.17$, giving $\langle k_{n+1} - k_n\rangle L_T = 3.15$. The corresponding numbers for the $N = 16$ graph, with the set of bond lengths (1.37, 1.39, 1.39, 1.43, 1.65, 1.72, 2.04, 2.25, 2.31, 2.45, 2.63, 2.85, 3.11, 3.25, 3.61, 3.61, 3.64, 4.16, 4.38, 4.56, 4.56, 4.58, 4.85, and 4.88), are $M = 2075$, $k_1 = 0.22$, $k_M = 100.00$, $\langle k_{n+1} - k_n\rangle = 0.048$, $\langle k_{n+1} - k_n\rangle L_T = 3.50$. Thus, we see that the expected average spacing is realized.

We then construct histograms for the normalized node voltages for the set of eigenfunctions. These are displayed in Fig. 2(a) for the $N = 4$ graph and in Fig. 2(b) for the $N = 16$ graph. Also, plotted on each graph is a Gaussian distribution function fit to the measured variance of the mode voltages. It can be seen that the Gaussian is a good fit for the $N = 16$ case and not so good for the $N = 4$ case. We might expect the Gaussian to be a good fit based on experience with the eigenfunction of so-called ray-chaotic cavities in two and three dimensions. Here the statistics of values of the eigenfunctions are Gaussian as a consequence of the random plane-wave hypothesis. That is, the field at any point in the enclosed domain can be viewed as a random superposition of a large number of plane waves with random phases.

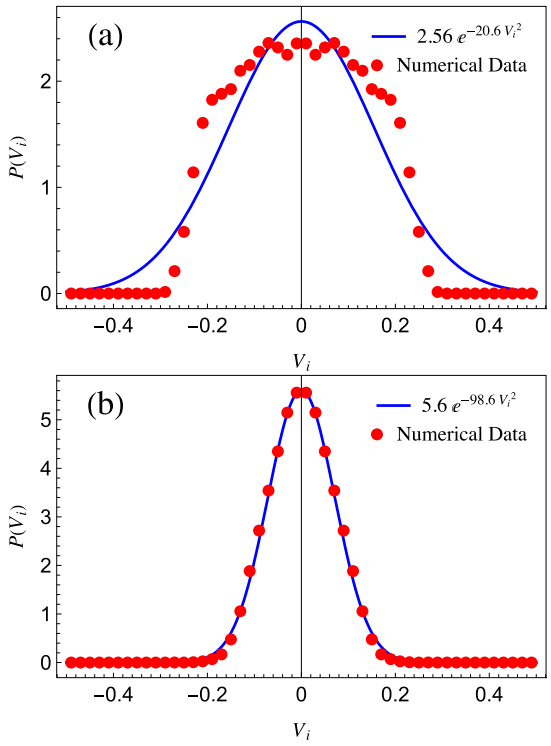

FIG. 2. Distribution functions of node voltage amplitudes for two different graphs. (a) Red dots show the distribution function of node voltage amplitudes for the tetrahedron graph: $N = 4$, $B = 3$. (b) Red dots show the distribution function of node voltage amplitudes for the larger graph: $N = 16$, $B = 3$. Blue lines are the Gaussian distribution functions fitted by minimizing the root-mean-square deviation between numerical data and the Gaussian fitting function in each case.

We now investigate the properties of the eigenvalue spectrum. The spectra of cable and waveguide networks have been studied previously [29,42]. In these studies, it was found that the distribution of spacings, $s_n = k_{n+1} - k_n$, was characteristic of systems described by random matrix theory (RMT) in that the spectrum exhibited level repulsion. However, it was also found that the spectra were more rigid (to be described) than RMT-like systems. Defining the normalized spacing $s_n = (k_{n+1} - k_n)/\langle k_{n+1} - k_n \rangle$, we make histograms of the values s_n. For this study, we add a reactance $Z_i = iX_i$ to the ground at each node, and we construct histograms for a number of values of the reactance. These are displayed in Fig. 3. The main effect of this reactance is to increase the reflection coefficient for a wave incident on a node according to Eq. (17). We note that for the lowest value of the reflection coefficient, the spacing distribution is well approximated by the spacing distribution of eigenvalues of a random matrix drawn from the Gaussian orthogonal ensemble, $P(s) = (\pi s/2)\exp(-\pi s/4)$. This is the distribution expected for eigenvalues of a wave chaotic cavity. We note from Fig. 3 that as the reflection coefficient at a node increases, the shape of the histogram changes, approaching a Poisson distribution $P(s) = \exp(-s)$ at the highest reflection value. This can be understood as follows. When the reflection coefficient becomes large, adjacent bonds become isolated from each other. The result is that

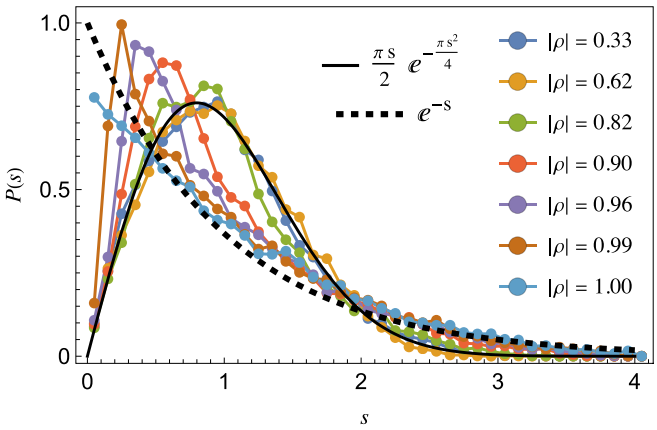

FIG. 3. Nearest-neighbor spacing distribution of normal mode wave vectors in tetrahedron graph ($N = 4$, $B = 3$), where $s = (k_{n+1} - k_n)/\langle k_{n+1} - k_n \rangle$. Shown for different reflection coefficients of the node, $|\rho|$. The solid line represents the spacing distribution of eigenvalues of a random matrix drawn from the Gaussian orthogonal ensemble. The dashed line is the Poisson distribution function.

the eigenvalues are determined by quantizing the individual bonds. The eigenvalues then fall uniformly distributed along the real k-line, and there is no level repulsion as exhibited in a wave chaotic cavity or as exhibited in a graph with strong coupling between bonds.

Varying the reflection coefficient also affects spectral rigidity. Here the spectral rigidity is characterized by the quantity

$$\Delta_3(L) = \langle \Delta_3(e; L) \rangle = \left\langle \frac{1}{L} \min_{A,B} \int_e^{e+L} [N(x) - Ax - B]^2 dx \right\rangle, \quad (19)$$

where $N(x)$ is the counting function that shows how many eigenvalues satisfy $|k_n| < x$.

Plots of $\Delta_3(L)$ as a function of interval length L and for different values of the reflection coefficient are shown in Fig. 4. The curves are qualitatively similar to those of Ref. [42]. Specifically, for small L, $\Delta_3(L)$ goes to zero, as it must based on its definition. It then increases with L and saturates once $L > 10$. In contrast, this quantity increases logarithmically with L for large L in wave chaotic systems. Thus, cable networks have more rigid spectra than wave chaotic systems. The main effect of varying the reflection coefficient

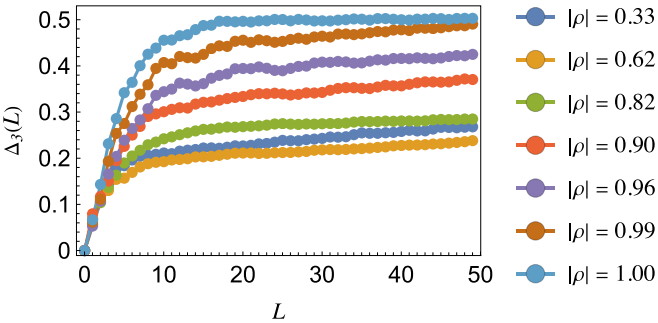

FIG. 4. Comparing $\Delta_3(L)$ statistics for different reflection coefficients, defined by Eq. (17), in a Tetrahedron graph ($N = 4$, $B = 3$).

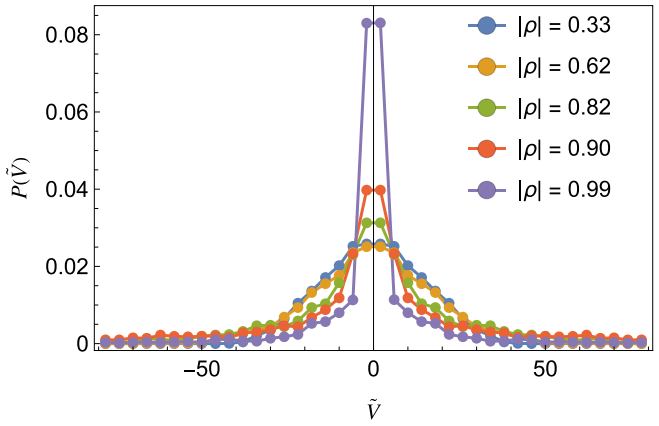

FIG. 5. Comparing statistics of node voltages (calculated only for one node) for different reflection coefficients, defined by Eq. (17), in a graph with $N = 16$, $N = 3$. Here node voltages are normalized by the variance of the node voltages. $\tilde{V} = V/\mathrm{var}[V]$.

is to vary the saturation value of $\Delta_3(L)$. For the case with the lowest reflection coefficient, the saturated value $\Delta_3(L \to \infty) = 0.2$, in agreement with Ref. [42]. For a perfect staircase with equal spacings, this value would be 0.125. As the reflection coefficient is raised, the saturated value $\Delta_3(L)$ increases. This can be understood as follows. As the reflection coefficient increases, the system approaches a collection of N_B, where N_B is the number of bonds, with isolated transmission lines of differing lengths. Thus, although each isolated bond has a perfect staircase spectrum, the composite spectrum will deviate from a perfect staircase, thus the higher value of saturated $\Delta_3(L)$.

It is also instructive the examine the effect of the reflection coefficient on the histograms of node voltages. This is illustrated in Fig. 5, where we plot histograms of node voltages normalized by the variance of the node voltages for different values of the reflection coefficient. (Notice the change in normalization). What is seen is that the histograms transition from what appears to be close to a normal distribution for the lowest reflection coefficient to histograms for which most nodes have low values of voltage while a few have large values of voltage. This can be understood again by considering the limit in which the network becomes an ensemble of isolated transmission lines. Depending on the eigenvalue, mode energy will be concentrated on the bond that is resonant. The nodes that terminate this bond will have large voltage values, while the other nodes will have small voltage values.

In Sec. II, we discussed that the impedance matrix could be calculated by inverting the admittance matrix or by representing the impedance matrix in terms of modes of the undriven network using Eq. (13). We now check that here. In principle, using Eq. (13) requires summing over all normal modes of the system. As this is not practical, we must truncate the sum. From the form of Eq. (13), we see that the representation of the impedance matrix will be accurate only for k-values in the middle of the range of the eigenvalues k_n of the modes retained in the sum. In Fig. 6, we show a comparison of the inverse of the admittance matrix and Eq. (13) for k-values in the range $249 < k < 251$. In the sum in Eq. (13) we have retained 2990

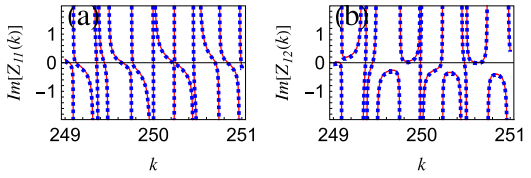

FIG. 6. Imaginary part of the (a) diagonal and (b) nondiagonal elements of the impedance matrix. The impedance values were determined in two ways: by inverting the admittance matrix [Eq. (9)] (red line) and by the sum over modes [Eq. (13)] (blue dots).

modes spanning the range of eigenvalues $0 < k < 500$. In this case, the agreement is quite good.

A second comparison can be made between the inverse of the admittance matrix and the summed contributions from the different paths a signal may take in traversing the graph, Eqs. (14) and (15). Similar to the case of Eq. (13), the infinite sums in Eqs. (14) and (15) will have to be truncated. In Fig. 7, we show comparisons between the inverse of the admittance matrix Eq. (8) and the path sums Eqs. (14) and (15) when the path sums have been truncated for lengths over six bonds. Impedance values are shown as functions of the real part of k for two different values of the imaginary part of k, and for two different graphs. Recall that evaluating the impedance with a complex k is equivalent to evaluating it for real k using a sliding Lorentzian window average for which the imaginary part of k defines the width of the window. Figure 7 shows that for small imaginary $k_{\mathrm{im}} = 0.03$, the truncated path sums only reproduce the coarse variations of the impedance. However, with larger $k_{\mathrm{im}} = 0.3$, the truncated sums agree quite well with the inverse of the admittance matrix. This is to be expected because for the two graphs, the average lengths of a bond are $\langle L_{ij} \rangle = 3.14$ and 3.03, respectively, for the $N = 4$ and 16 graphs. Evaluating the matrix with an imaginary k is equivalent to adding spatial damping to the waves propagating on the bonds. For the $N = 4$ case with $k_{\mathrm{im}} = 0.03$ we find $6k_{\mathrm{im}}\langle L_{ij} \rangle = 0.57$, and with $k_{\mathrm{im}} = 0.3$ we find $6k_{\mathrm{im}}\langle L_{ij} \rangle = 5.7$. Similarly, for the $N = 16$ case with $k_{\mathrm{im}} = 0.03$ we find $6k_{\mathrm{im}}\langle L_{ij} \rangle = 0.55$, and with $k_{\mathrm{im}} = 0.3$ we find $6k_{\mathrm{im}}\langle L_{ij} \rangle = 5.5$.

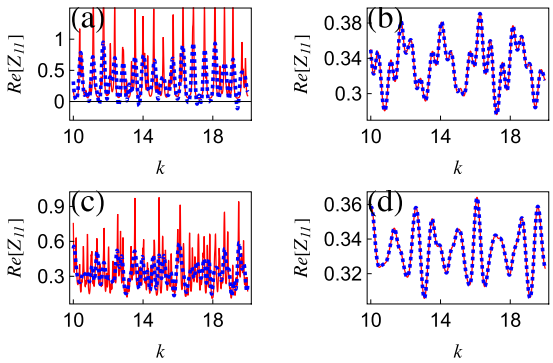

FIG. 7. Comparison between the inverse of the admittance matrix (red line) and summed contributions (blue dots) from the different paths a signal may take in traversing the graph. Tetrahedron graph ($N = 4$, $B = 3$) using (a) $k_{\mathrm{im}} = 0.03$ and (b) $k_{\mathrm{im}} = 0.3$. Larger graph ($N = 16$, $B = 3$) using (c) $k_{\mathrm{im}} = 0.03$ and (d) $k_{\mathrm{im}} = 0.3$. In all cases, we used all paths up to and including six bonds.

Thus, the contributions from six paths are sufficient for the $k_{\rm im} = 0.3$ case, but not in the $k_{\rm im} = 0.03$ case.

We now investigate the distribution of impedance values for networks of varying sizes. We focus on the variance of the imaginary part of the elements of networks with $N = 4$, 8, and 16 nodes. We also consider two values of the number of bonds per node (the degree) $B = 3$ and 5. We choose to characterize the imaginary part of the impedance as opposed to the real part, as it has zero mean and a distribution function of even symmetry. The statistics of the real part of the diagonal elements are complicated by the fact that the real part is positive-definite and has a nonzero mean. The mean value of the real part of a diagonal element is independent of the loss rate. When the loss rate is small, the distribution of values of the real part of a diagonal element becomes skewed in the sense that there is a large probability of a small real value and a small probability of a large value.

We computed the imaginary part of the diagonal and nondiagonal impedance elements of 20 realizations of networks of varying size, each for 49 980 values of k, and with varying loss rate $k_{\rm im}$. We then attempted to find universal scaling relations that characterized the variance. The variance of the imaginary part of diagonal elements scaled by N^p, $\mathrm{var}\,(\mathrm{Im}(Z_{11}))N^p$, where p is adjusted to make the curves fall on top of each other. We find $p = -0.3$ for graphs with $B = 3$ and $p = -0.4$ for graphs with $B = 5$. The variance of the imaginary part of nondiagonal elements, each averaged over 49 980 values of k, is plotted versus $k_{\rm im} \sum L_{ij}$ in Figs. 8(a) and 8(b), respectively. Here $\sum L_{ij}$ is the total length of a graph. We find that scaling by N^p for diagonal elements, and by plotting versus $k_{\rm im} \sum L_{ij}$, results from networks of different sizes and degrees falling on top of each other. This is true for both large and small values of damping, as indicated in the figure and its inset. The scaling with $k_{\rm im} \sum L_{ij}$ is similar to that obtained for two- and three-dimensional cavities. For cavities, the relevant measure of damping is the loss rate normalized to the mean spacing between modes. The averaged spacing between modes for these network is $\langle k_{n+1} - k_n \rangle = \pi / L_T$, where $L_T = \sum L_{ij}$. Thus, these networks exhibit the expected dependence on $k_{\rm im} \sum L_{ij}$, where $\sum L_{ij}$ is the total length of the bonds. Furthermore, we checked how the actual distribution functions compare to each other when we have the universal scaling relations that characterize their variances. In Fig. 8, we can see that for $k_{\rm im} \sum L_{ij} = 1.5$, the variances of diagonal elements of the impedance matrix scaled by N^p fall on top of each other, and also, the same happens to the variances of nondiagonal elements. To exclude the scaling factor that is used for diagonal elements of the impedance matrix, we compared the distribution functions of diagonal elements of the impedance matrix scaled by $1/\sqrt{N^p}$. Eventually, we found out that as long as their variances are very close, their distributions do not fall on top of each other. The results are provided in Fig. 9.

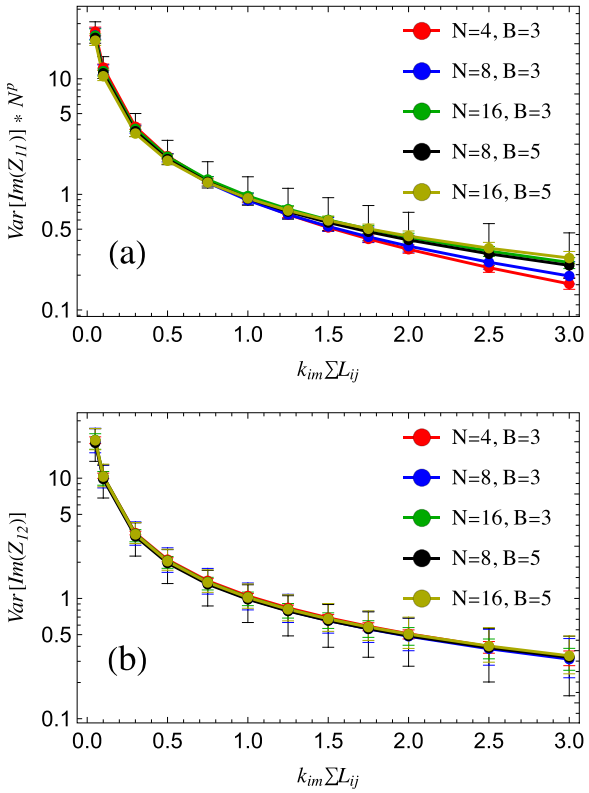

FIG. 8. (a) The variance of the imaginary part of diagonal elements of the impedance matrix scaled by N^p, where N is the total number of nodes and $p = -0.3$ for graphs with $B = 3$ and $p = -0.4$ for graphs with $B = 5$, and (b) nondiagonal elements plotted vs $k_{\rm im} \sum L_{ij}$. There are five different-sized graphs, each curve represents the result averaged over 20 different realizations, and error bars on each plot point represent the range in which the values vary during all realizations.

IV. COMPARISON WITH MEASURED IMPEDANCES

We now compare predicted impedance statistics with those measured on a network of cables. The experimental configuration is described extensively in Refs. [1,12,24,43–45]. It consists of a tetrahedral network ($N = 4, B = 3$) of 50 Ohm coaxial cables of varying lengths. These cables are connected at nodes using T-junctions. Comparisons between our simulations and measured [45] impedance values are displayed in Fig. 10. For these comparisons, we simulated a tetrahedral graph ($N = 4, B = 3$) for which we choose bond lengths that correspond to those in the experiment. In the experimental setup, the nodes are not grounded through an impedance, thus we set Z_i to infinity in the first numerical calculations.

To compare numerical results with that measured [45], we need to determine an attenuation rate $k_{\rm im}$ on the bonds. The calculated and measured attenuation rate on the coaxial cables is presented in Appendix B of Ref. [45] as a function of frequency. The authors of Ref. [45] found that the attenuation varies with frequency. We thus select data in two ranges, 6–9 and 12–15 GHz, in which the variation of the attenuation rate with frequency is approximately linear. In the simulations we used $0.129 < k_{\rm im} < 0.165\ \mathrm{m}^{-1}$ for $6 < f < 9$ GHz and $0.198 < k_{\rm im} < 0.228\ \mathrm{m}^{-1}$ for $12 < f < 15$ GHz. Results for impedance values in the form of histograms are shown in Fig. 10(a) for frequencies in the 6–9 GHz range and in Fig. 10(b) for frequencies in the 12–15 GHz range. There are four panels for the real and imaginary parts of the diagonal and off-diagonal elements of the impedance matrix. For each case, there are 84 different realizations of the network using bonds of different lengths, and for each realization, the data

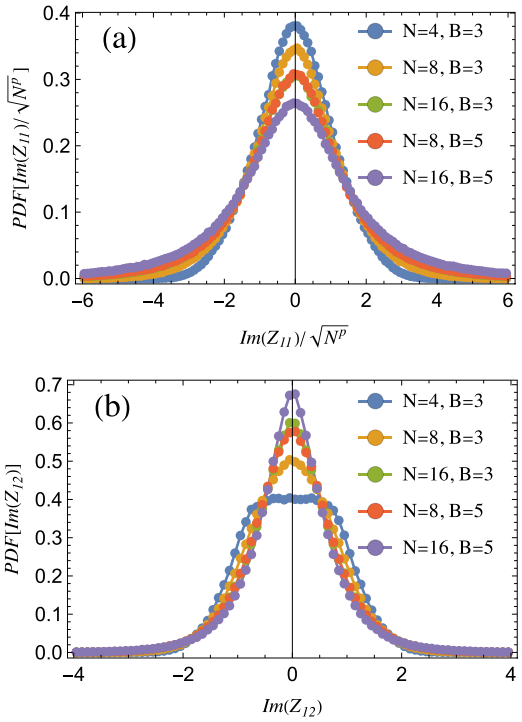

FIG. 9. The distribution functions of the imaginary part of (a) diagonal elements of impedance matrix scaled by $1/\sqrt{N^p}$, where N is the total number of nodes and $p = -0.3$ for graphs with $B = 3$ and $p = -0.4$ for graphs with $B = 5$, and (b) nondiagonal elements. These data correspond to $k_{\rm im} \sum L_{ij} = 1.5$. There are five different-sized graphs. Each curve represents the result averaged over 20 different realizations.

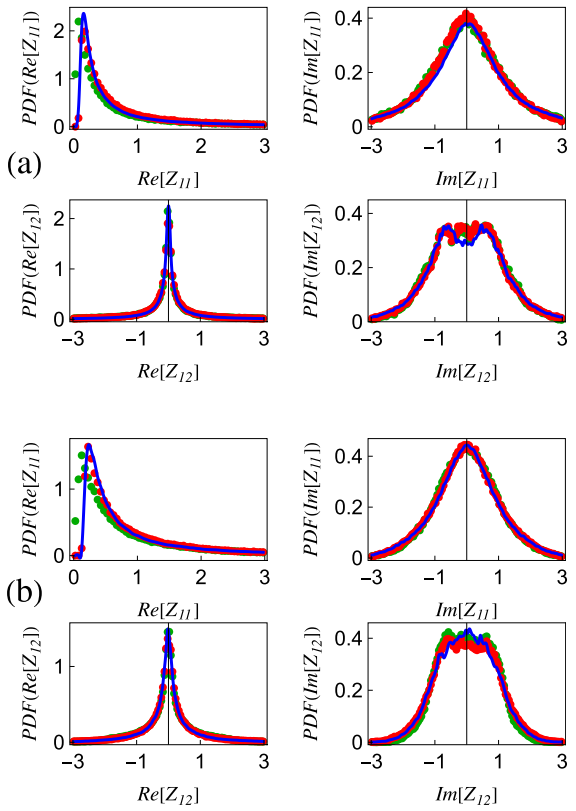

FIG. 10. Comparison between histograms of numerically generated impedance matrix elements and experimentally measured values for an $N = 4, B = 3$ graph. (a) Loss is modeled in two different ways: using Eqs. (9a) and (9b) with $Z_i = 4.0$ and $k_{\rm im} = 0.0$ (green dots) and using Eqs. (9a) and (9b) with $Z_i = \infty$ and $k_{\rm im} \in [0.129, 0.165]$ changing linearly (red dots). Experimental data (blue line) were produced for the frequency range of 6–9 GHz, and corresponding $k_{\rm im}$ changes linearly from 0.129 to 0.165. (b) Loss is modeled in two different ways: using Eqs. (9a) and (9b) with $Z_i = 2.6$ and $k_{\rm im} = 0.0$ (green dots) and using Eqs. (9a) and (9b) with $Z_i = \infty$ and, $k_{\rm im} \in [0.198, 0.228]$ changing linearly (red dots). Experimental data (blue line) were produced for the frequency range of 12–15 GHz, and corresponding $k_{\rm im}$ changes linearly from 0.198 to 0.228.

are generated by changing wave-vector value (essentially the frequency).

To investigate the dependence on the type of loss, we have added to Fig. 10 calculated impedance values assuming the cables are lossless, but instead there are real impedance elements connecting the nodes to the ground. The value of this impedance was adjusted to match the other histograms, $Z_i = 4.0$ for $f = 6$–9 GHz and $Z_i = 2.7$ for $f = 12$–15 GHz. Note that the lossy element connects a node to ground, so a larger value of Z_i corresponds to lower loss. As can be seen, the three types of histograms (experiment, distributed loss simulated, and localized loss simulated) are quite similar. This includes the multiple peaks in the $\mathrm{Im}(Z_{12})$ histograms, which are due to direct paths from port 1 to port 2, as discussed below.

Previously [1], the impedance statistics of this configuration were compared with predictions of the RCM. It was found that the statistics of the nondiagonal and diagonal elements of the impedance matrix required fitting with different loss factors to obtain agreement. Generally, the diagonal elements required higher loss than the off-diagonal elements to obtain a fit. Our purpose here is to determine whether this is a feature of these networks reproduced by our simple model. What we have found is that the histograms of the diagonal and nondiagonal elements are matched to the experimental histograms by the same loss parameter. Thus, the network is not modeled by the RCM. In Sec. I, we have described three different ways to compute the impedance matrix. We found the most straightforward way to calculate the impedance matrix accurately is to invert the admittance matrix given by Eq. (9), which results in Eq. (10). In general, the random coupling model (RCM) describes the systems without short-orbit [46] contributions. Therefore, to compare our results to the RCM, we should ensure that we have excluded short-orbit contributions from the calculations. For that purpose, we can recall that we have discussed how to calculate the impedance matrix based on summing contributions from the different paths, $Z_{ij,\rm path}$, and this was described by Eqs. (14) and (15). However, if we use a finite number of paths in $Z_{ij,\rm path}$, we can generate only the short-orbit contributions in the impedance matrix. Afterward, we can subtract these contributions from the impedance matrix calculated using Eq. (10), which results in the redefined impedance matrix without short-orbit contributions,

$$\hat{Z}_{ij}(k) = [Y(k)]^{-1}_{ij} - Z_{ij,\rm path}(k). \tag{20}$$

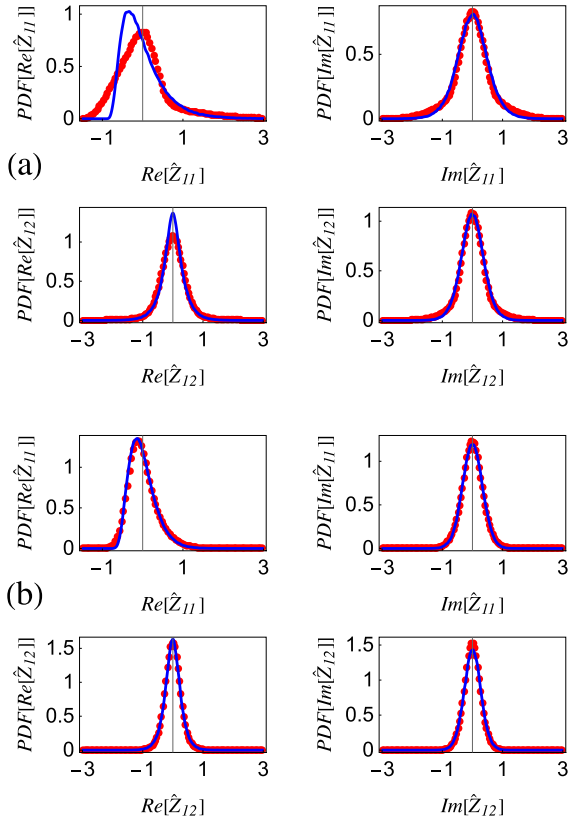

FIG. 11. Comparing impedance matrix distribution function elements, calculated by Eq. (20), to RCM. (a) Equation (20) (red dots) has used the graph with $N = 4$, $B = 3$, and $k_{\rm im} = 0.03$ in all cases; RCM (blue line) has used $\alpha = 1.20$ for diagonal elements and $\alpha = 1.00$ for nondiagonal elements. (b) Equation (20) (red dots) has used the graph with $N = 16$, $B = 3$, and $k_{\rm im} = 0.03$ in all cases; RCM (blue line) has used $\alpha = 3.00$ for diagonal elements and $\alpha = 1.90$ for nondiagonal elements.

We generated data for two different networks, $(N = 4, B = 3)$ and $(N = 16, B = 3)$. We set a fixed loss rate, $k_{\rm im} = 0.03$, for both of the cases and varied α, the loss parameter in the RCM. We found out that the statistics of the redefined impedance matrix for the $(N = 4, B = 3)$ network, calculated by Eq. (20), and the RCM have the best agreement when $\alpha = 1.20$ and 1.00 for diagonal and nondiagonal elements, respectively. The corresponding results for the $(N = 16, B = 3)$ network are $\alpha = 3.00$ and 1.90 for diagonal and nondiagonal elements, respectively. The results are shown in Fig. 11.

Our findings are consistent with those described in [1] based on measurements. The predicted distributions of values of the elements of the impedance matrix based on our model agree with those measured. However, as in [1], the distributions of impedance values from our model, when fit to the RCM, require different values of loss to fit the diagonal and off-diagonal elements. A possible cause for this discrepancy is the nonvanishing reflection seen by a wave propagating on a bond and incident on a node. Given our model of the nodes, the smallest magnitude of the voltage reflection coefficient can be 1/3. This reflection is absent in 2D and 3D cavities for which good agreement with the RCM is attained. We have found that increasing this reflection coefficient causes the mode eigenfrequency spacing statistics to transition from a GOE-like distribution to a Poisson-like distribution. Thus, the small reflection may be responsible for the deviations from RCM statistics. A recent study [32,40] has modeled the nodes using a scattering matrix based on a Fourier decomposition of the elements. Such a representation allows for the reflection to be eliminated, and the authors find agreement with RCM statistics. Implementing such a scattering matrix in an experiment is a challenge. Various matching techniques can be considered. However, these are usually effective only over a limited range of frequencies, making generating a large ensemble of impedance values difficult.

V. CONCLUSION

In this work, we have obtained several interesting results. We found that by changing the values of the reflection coefficients at the nodes, we can change the statistics of the distribution of normal-mode wave-vector spacings. This is shown in Fig. 3. We have shown that the results of the developed framework adequately reproduce the experimental results; see Fig. 10. We also have presented three different approaches to calculating the impedance matrix: one that is precise, one that is based on summing over the normal modes of the graph, and one that is based on summing over paths through the graph. We compared these approaches and determined the circumstances under which they agreed. Finally, we showed that there is a universal formula for the dependence of the size of the fluctuations of $\mathrm{Im}(Z_{11})$ on the propagation loss rate and the number of nodes in the graph. The dependence is given in Fig. 8.

ACKNOWLEDGMENTS

This work was supported by AFOSR/AFRL under FA9550-15-1-0171 and ONR under N000141912481.

APPENDIX: NORMAL MODES AND THE IMPEDANCE MATRIX

To find the relation between normal modes and the impedance matrix, which for a driven system $I_j \neq 0$ is defined for all values of propagation constant k, we first multiply the Telegrapher's equations by the conjugate of a mode voltage and current, respectively, integrate in z over each bond, add the two equations, and sum over bonds,

$$i(k-k_n)\sum_{ij}\int_0^{L_{ij}} dz\big(Z_0^{-1}V^{(n)^*}V(z)+Z_0 I^{(n)^*}(z)I(z)\big)$$
$$=\sum_{ij}(V^{(n)^*}I(z)+V(z)I^{(n)*})|_0^{L_{ij}}. \tag{A1}$$

The right-hand side involves the evaluation of voltages and currents at nodes, and it can be converted into a sum over nodes. Each node will enter twice, first as the lower limit, $(z = 0)$, and second as the upper limit, $(z = L_{ij})$. The current variables have opposite meanings in these cases. At $z = 0$, the current variables represent the currents leaving a node, and at $z = L_{ij}$ they represent the currents entering a node. Thus we write both in terms of the currents leaving node-i in the

direction of node-j,

$$\sum_{ij}(V^{(n)^*}I(z)+V(z)I^{(n)*})|_0^{L_{ij}}$$

$$=-2\left(\sum_{\text{nodes-}i}V_i^{(n)^*}\sum_{ij}I_{i\to j}+\sum_{\text{nodes-}i}V_i\sum_{ij}I_{i\to j}^{(n)^*}\right). \quad \text{(A2)}$$

The value of the sum of the currents leaving a node will depend on whether the current variables apply to a normal mode or a driven solution. In the case of a normal mode with an index m,

$$\sum_{ij}I_{i\to j}^{(m)}+\frac{V_i^{(m)}}{Z_i}=0. \quad \text{(A3)}$$

Thus, if we consider the loss-free case $Z_i^*=-Z_i$, the two terms cancel. As a result,

$$i(k-k_n)\sum_{ij}\int_0^{L_{ij}}dz\big(Z_0^{-1}V^{(n)^*}(z)V^{(m)}(z)$$

$$+Z_0I^{(n)^*}(z)I^{(m)}(z)\big)=0, \quad \text{(A4)}$$

and we conclude that the modes represent an orthogonal basis. In the case of a driven solution,

$$\sum_{ij}I_{i\to j}^{(m)}+\frac{V_i^{(m)}}{Z_i}=I_i, \quad \text{(A5)}$$

and we obtain

$$i(k-k_n)\sum_{ij}\int_0^{L_{ij}}dz\big(Z_0^{-1}V^{(n)^*}V(z)+Z_0I^{(n)^*}(z)I(z)\big)$$

$$=-2\left(\sum_{\text{nodes-}i}V_i^{(n)^*}I_i\right). \quad \text{(A6)}$$

We now expand the voltages and currents on the transmission lines in a superposition of voltages and currents corresponding to normal modes,

$$(V(z),I(z))=\sum_m C_m(V^{(m)}(z),I^{(m)}(z)). \quad \text{(A7)}$$

Using the orthogonality property, we find for the coefficients C_n,

$$i(k-k_n)C_n=\frac{-2\left(\sum_{\text{nodes-}i}V_i^{(n)^*}I_i\right)}{\sum_{ij}\int_0^{L_{ij}}dz\left(Z_0^{-1}\left|V^{(n)}\right|^2+Z_0\left|I^{(n)}\right|^2\right)}. \quad \text{(A8)}$$

Consequently, we can express the voltage at a node in the driven case in terms of the impedance matrix, which in turn is expressed in terms of the normal modes.

[1] Z. Fu, T. Koch, T. M. Antonsen, E. Ott, and S. M. Anlage, Experimental study of quantum graphs with simple microwave networks: Non-universal features, Acta Phys. Pol. A **132**, 1655 (2017).

[2] S. Gnutzmann and U. Smilansky, Quantum graphs: Applications to quantum chaos and universal spectral statistics, Adv. Phys. **55**, 527 (2006).

[3] D. Kowal, U. Sivan, O. Entin-Wohlman, and Y. Imry, Transmission through multiply-connected wire systems, Phys. Rev. B **42**, 9009 (1990).

[4] Z. Pluhař and H. A. Weidenmüller, Universal Quantum Graphs, Phys. Rev. Lett. **112**, 144102 (2014).

[5] T. Kottos and U. Smilansky, Quantum Chaos on Graphs, Phys. Rev. Lett. **79**, 4794 (1997).

[6] B. Dietz and A. Richter, Intermediate statistics in singular quarter-ellipse shaped microwave billiards, J. Phys. A **55**, 314001 (2022).

[7] E. L. Ivchenko and A. A. Kiselev, Electron g factor in quantum wires and quantum dots, J. Exp. Theor. Phys. Lett. **67**, 43 (1998).

[8] J. A. Sánchez-Gil, V. Freilikher, I. Yurkevich, and A. A. Maradudin, Coexistence of Ballistic Transport, Diffusion, and Localization in Surface Disordered Waveguides, Phys. Rev. Lett. **80**, 948 (1998).

[9] Y. Imry, *Introduction to Mesoscopic Physics*, 2nd ed. (Oxford University Press on Demand, 2002).

[10] R. Mittra, *Analytical Techniques in the Theory of Guided Waves*, Macmillan Series in Electrical Science (Macmillan, 1971).

[11] S. Ma and S. M. Anlage, Microwave applications of photonic topological insulators, Appl. Phys. Lett. **116**, 250502 (2020).

[12] O. Hul, O. Tymoshchuk, S. Bauch, P. M. Koch, and L. Sirko, Experimental investigation of wigner's reaction matrix for irregular graphs with absorption, J. Phys. A **38**, 10489 (2005).

[13] L. Pauling, The diamagnetic anisotropy of aromatic molecules, J. Chem. Phys. **4**, 673 (1936).

[14] S. Gnutzmann and A. Altland, Universal Spectral Statistics in Quantum Graphs, Phys. Rev. Lett. **93**, 194101 (2004).

[15] M. L. Mehta, *Random Matrices* (Elsevier, Amsterdam, 2004).

[16] J. Lu, J. Che, X. Zhang, and B. Dietz, Experimental and numerical investigation of parametric spectral properties of quantum graphs with unitary or symplectic symmetry, Phys. Rev. E **102**, 022309 (2020).

[17] V. Yunko, M. Białous, and L. Sirko, Edge switch transformation in microwave networks, Phys. Rev. E **102**, 012210 (2020).

[18] J. Che, J. Lu, X. Zhang, B. Dietz, and G. Chai, Missing-level statistics in classically chaotic quantum systems with symplectic symmetry, Phys. Rev. E **103**, 042212 (2021).

[19] M. Białous, V. Yunko, S. Bauch, M. Ławniczak, B. Dietz, and L. Sirko, Power Spectrum Analysis and Missing Level Statistics of Microwave Graphs with Violated Time Reversal Invariance, Phys. Rev. Lett. **117**, 144101 (2016).

[20] M. Ławniczak, M. Białous, V. Yunko, S. Bauch, B. Dietz, and L. Sirko, Analysis of missing level statistics for microwave networks simulating quantum chaotic graphs without time reversal symmetry-the case of randomly lost resonances, Acta Phys. Pol. A **132**, 1672 (2017).

[21] M. Białous, B. Dietz, and L. Sirko, Missing-level statistics in a dissipative microwave resonator with partially violated time-reversal invariance, Phys. Rev. E **103**, 052204 (2021).

[22] C. H. Joyner, S. Müller, and M. Sieber, GSE statistics without spin, Europhys. Lett. **107**, 50004 (2014).

[23] A. Rehemanjiang, M. Allgaier, C. H. Joyner, S. Muller, M. Sieber, U. Kuhl, and H. J. Stockmann, Microwave Realization of the Gaussian Symplectic Ensemble, Phys. Rev. Lett. **117**, 064101 (2016).

[24] O. Hul, S. Bauch, P. Pakoński, N. Savytskyy, K. Życzkowski, and L. Sirko, Experimental simulation of quantum graphs by microwave networks, Phys. Rev. E **69**, 056205 (2004).

[25] M. Ławniczak, S. Bauch, O. Hul, and L. Sirko, Experimental investigation of the enhancement factor for microwave irregular networks with preserved and broken time reversal symmetry in the presence of absorption, Phys. Rev. E **81**, 046204 (2010).

[26] O. Hul, M. Ławniczak, S. Bauch, A. Sawicki, M. Kuś, and L. Sirko, Are Scattering Properties of Graphs Uniquely Connected to Their Shapes? Phys. Rev. Lett. **109**, 040402 (2012).

[27] M. Allgaier, S. Gehler, S. Barkhofen, H.-J. Stöckmann, and U. Kuhl, Spectral properties of microwave graphs with local absorption, Phys. Rev. E **89**, 022925 (2014).

[28] M. Ławniczak, S. Bauch, O. Hul, and L. Sirko, Experimental investigation of properties of hexagon networks with and without time reversal symmetry, Phys. Scr. **2009**, 014050 (2009).

[29] B. Dietz, V. Yunko, M. Białous, S. Bauch, M. Ławniczak, and L. Sirko, Nonuniversality in the spectral properties of time-reversal-invariant microwave networks and quantum graphs, Phys. Rev. E **95**, 052202 (2017).

[30] S. Hemmady, T. M. Antonsen, E. Ott, and S. M. Anlage, Statistical prediction and measurement of induced voltages on components within complicated enclosures: A wave-chaotic approach, IEEE Trans. Electromagn. Compatibil. **54**, 758 (2012).

[31] M. Ławniczak, O. Hul, Sz. Bauch, and L. Sirko, Experimental and numerical studies of one-dimensional and three-dimensional chaotic open systems, Acta Phys. Pol. A **116**, 749 (2009).

[32] M. Ahmed, G. Gradoni, S. Creagh, C. Smartt, S. Greedy, and G. Tanner, Energy transfer in complex networks: A quantum graph approach, in *2019 International Conference on Electromagnetics in Advanced Applications (ICEAA)* (IEEE, Piscataway, NJ, 2019), pp. 1231–1234.

[33] M. Ahmed, G. Gradoni, S. Creagh, C. Smartt, S. Greedy, and G. Tanner, Transport of power through networks of cables using quantum graph theory, in *2019 International Symposium on Electromagnetic Compatibility-EMC EUROPE* (IEEE, Piscataway, NJ, 2019), pp. 820–824.

[34] G. Gradoni, J.-H. Yeh, B. Xiao, T. M. Antonsen, S. M. Anlage, and E. Ott, Predicting the statistics of wave transport through chaotic cavities by the random coupling model: A review and recent progress, Wave Motion **51**, 606 (2014).

[35] S. Hemmady, X. Zheng, E. Ott, T. M. Antonsen, and S. M. Anlage, Universal Impedance Fluctuations in Wave Chaotic Systems, Phys. Rev. Lett. **94**, 014102 (2005).

[36] Z. Drikas, J. G. Gil, S. K. Hong, T. Andreadis, J. H. Yeh, B. T. Taddese, and S. M. Anlage, Application of the random coupling model to electromagnetic statistics in complex enclosures, IEEE Trans. Electromagn. Compatibil. **56**, 1480 (2014).

[37] J. Gil Gil, Z. B. Drikas, T. D. Andreadis, and S. M. Anlage, Prediction of induced voltages on ports in complex, three-dimensional enclosures with apertures, using the random coupling model, IEEE Trans. Electromagn. Compatibil. **58**, 1535 (2016).

[38] S. Ma, S. Phang, Z. Drikas, B. Addissie, R. Hong, V. Blakaj, G. Gradoni, G. Tanner, T. M. Antonsen, E. Ott, and S. M. Anlage, Efficient Statistical Model for Predicting Electromagnetic Wave Distribution in Coupled Enclosures, Phys. Rev. Appl. **14**, 014022 (2020).

[39] S. Ma, B. Xiao, Z. Drikas, B. Addissie, R. Hong, T. M. Antonsen, E. Ott, and S. M. Anlage, Wave scattering properties of multiple weakly coupled complex systems, Phys. Rev. E **101**, 022201 (2020).

[40] M. Ahmed, G. Gradoni, S. Creagh, C. Smartt, S. Greedy, and G. Tanner, Distribution of energy through cable networks using random coupling model, in *2020 International Symposium on Electromagnetic Compatibility-EMC EUROPE* (IEEE, Piscataway, NJ, 2020), pp. 1–6.

[41] G. Berkolaiko and P. Kuchment, *Introduction to Quantum Graphs*, Vol. 186 (American Mathematical Society, 2013).

[42] S. Ma, T. M. Antonsen, and S. M. Anlage, Eigenfunction and eigenmode-spacing statistics in chaotic photonic crystal graphs, Phys. Rev. E **106**, 054215 (2022).

[43] L. Chen, T. Kottos, and S. M. Anlage, Perfect absorption in complex scattering systems with or without hidden symmetries, Nat. Commun. **11**, 5826 (2020).

[44] L. Chen, S. M. Anlage, and Y. V. Fyodorov, Generalization of wigner time delay to subunitary scattering systems, Phys. Rev. E **103**, L050203 (2021).

[45] L. Chen and S. M. Anlage, Use of transmission and reflection complex time delays to reveal scattering matrix poles and zeros: Example of the ring graph, Phys. Rev. E **105**, 054210 (2022).

[46] J. A. Hart, T. M. Antonsen Jr, and E. Ott, Effect of short ray trajectories on the scattering statistics of wave chaotic systems, Phys. Rev. E **80**, 041109 (2009).